Discrete-Time Tool for Stability Analysis of DC Power Electronics Based Cascaded Systems

Mehdi Karbalaye Zadeh, *Student Member, IEEE*, Roghayeh Gavagsaz-Ghoachani, Jean-Philippe Martin, Serge Pierfederici, Babak Nahid-Mobarakeh, *Senior Member, IEEE*, and Marta Molinas, *Member, IEEE*

Abstract— **DC distribution power systems are vulnerable to instability because of the destabilizing effect of converter-controlled constant power loads (CPLs) and input filters. Standard stability analysis tools based on averaging linearization techniques can be used only when the switching frequency of the converter is significantly higher than the cutoff frequency of the filter. However, DC distribution systems with a reduced size filter, and consequently a high cutoff frequency, are common in transportation applications. Conventional methods fail to detect instabilities in the system because they do not take into account the switching effect. To overcome this drawback, this paper proposes a discrete-time method to analyze the stability of DC distribution systems. This model is applied here to a DC power system with a constant power load. The switching effects and nonlinearities of the system model are taken into account with a simple discretization approach. The proposed method is able to predict the dynamic properties of the system, such as slow scale and fast scale instabilities. An active stabilizer is also included in the system model in order to extend the stability margin of the system. Finally, these observations are validated experimentally on a laboratory test-bench.**

Index Terms—**Dc microgrids, stability, discrete-time modeling, digital control, nonlinear systems, bifurcation, dc-dc converters.**

I. INTRODUCTION

DEVELOPMENTS in power electronics technologies have resulted in an increasing use of electronically controlled power generations and loads in both AC and DC networks [1-5]. Despite the trends in AC microgrids during the past decade, DC distribution has become of special interest for electric and hybrid electric vehicles, electric ships and more electric aircraft (MEA) [6-8]. However, instability is still a major issue in the design of DC power systems. It arises from the nonlinear characteristics of power electronics systems,

which can lead to unstable oscillations and potential routes to chaos [9-11]. These oscillations may be initiated either by the interactions between the controllers and the nonlinear switching effect of the converters, or by the constant power dynamics of tightly regulated active loads [11]. Such loads are usually controlled by pulse width modulated (PWM) converters, where the control bandwidth of the load converters is sufficiently high to ensure that the regulated load power is not influenced by fluctuations in DC bus voltage [6]. This introduces a negative impedance characteristic at the load terminal [12]. In stability studies, the load converters are usually modeled as constant power loads (CPLs) [12-22]. Interaction between DC power systems and the nonlinear characteristics of CPLs can lead to instability [12, 13]. CPL instability has been studied using small-signal stability analysis, such as modal analysis and participation factor analysis [14-16]. Linear and nonlinear controllers have been compared based on their trajectories in phase portraits, and this approach was used to study limit cycle oscillations in a simplified DC system with CPL [17]. CPL instability has also been studied by large signal stability analysis involving estimation of the domain of attraction using Lyapunov linearization and mixed potential theory [18-21]. In addition, the existence of equilibrium has been studied for an N-port system with CPLs in [22].

Most research on the stability of DC power systems is based on averaged linearization techniques: an averaged model of the individual converters is used in the model of the system [23-25]. The resulting averaged models are then used to obtain a small signal model of the system, usually as impedance expression. The impedance-based method was first proposed to study the dynamic behavior of DC-DC converters in [26], and became the first step in the stability analysis of distributed power systems. In this method, the system is divided into a source and a load sub-system, and the stability of the system is determined by the ratio of the source output impedance to the load input impedance for the interconnected source-load system [27-29]. Although specifying the impedance usually guarantees the stable design of an individual load, such methods cannot give an accurate stability region, because of the interactive dynamics of the system [30]. Moreover, the resulting model is nonlinear not only because of the nonlinear nature of switching converters, but also because of the load dynamics. Therefore, if small-signal linearization is used, the dynamic characteristics of the system are neglected.

To avoid small-signal linearization, numerical simulation is used to study the behavior of the system with nonlinear tools

M. Karbalaye Zadeh is with the Department of Electric Power Engineering, Norwegian University of Science and Technology, Trondheim 7491, Norway (e-mail: mehdi.zadeh@ntnu.no).

R. Gavagsaz-Ghoachani, J-P. Martin, S. Pierfederici, and B. Nahid-Mobarakeh are with the Groupe de Recherche en Électrotechnique et Électronique de Nancy, Ecole Nationale Supérieure d'Électricité et de Mécanique, Université de Lorraine, Nancy 54000, France (e-mail: roghayeh.gavagsazghoachani@univ-lorraine.fr; jean-philippe.martin@univ-lorraine.fr; serge.pierfederici@univ-lorraine.fr; babak.nahidmobarakeh@univ-lorraine.fr).

M. Molinas is with the Department of Engineering Cybernetics, Norwegian University of Science and Technology, Trondheim 7491, Norway (e-mail: marta.molinas@ntnu.no).

including phase portraits, Lyapunov, and bifurcation [31]. Nevertheless, qualitative studies, such as analyzing the sensitivity of the system's state to the variation of parameters and predicting the stability margin, necessitate system modeling. On the other hand, the continuous-time averaging or averaged models, which are the basis of classical methods, neglect the impact of the switching frequency. For this reason, such models are valid only if the switching frequency is much higher than the natural resonant frequencies of the system [32]. However, when the size of the filter is reduced, the resonant frequency increases. Therefore, classical tools cannot accurately study the stability margin, neither the dynamic behavior of the system.

Discrete-time models are a reliable solution to study the dynamic behavior of switching converters [33-39]. The discritization approach has been mainly used for control design. An improvement in the application of discretization approach was made in [33], and the method was developed to design an optimal control for a DC converter in [34]: the switching period was divided into υ subperiods, namely υ-resolution hybrid model; the exponential matrices were calculated over each subperiod; the accuracy of the υ-resolution was then investigated by changing υ (Fig. 3 in [34]). In that work, the physical system was formulated by a hybrid function comprised of piecewise functions. This is a solution to take into account the discrete properties of the controller. Lyapunov stability analysis was also performed for the presented controller using a piecewise quadratic Lyapunov as a function of the state trajectory (Fig. 6 in [33]). That method was advantageous over the previous techniques, since the exponential terms were calculated for each subperiod and the accuracy of the model was increased. Discrete-time solutions are a successful approach to study the nonlinear dynamics of a single converter [35-38]. However, previous discrete-time models are very complex because the exponential matrices and integral terms are involved in the formulation of the physical model. Hence, the use of such methods has not been extended to practical applications with CPLs. One study combined discrete-time and averaging approach to avoid exact discrete modeling [39]. However, the model was partially frequency-dependent because of the averaging integrals, and discretization was still based on the time-series solution.

In this paper, an exact discrete-time tool is proposed to analyze the stability of such DC distribution systems in different operation modes of the system. In the proposed method, the switching frequency and the nonlinear dynamics of the system model are taken into account by developing a discrete-time model of the complete system. The switching period is really discretized using a general and nonlinear discretization method, which is applicable to various types of PWM converters. The digital PWM controller is then taken into the system model using two series of state variables such as physical variables and control variables. After obtaining the discrete-time model, stability of the system can be investigated by calculating the eigenvalues of the discrete-time Jacobian matrix, and by constructing bifurcation diagram [40, 41].

The proposed method is applied to predict the system's instability using the eigenvalues, and to study the dynamic behavior of the system using bifurcation analysis. We prove

that the instability can occur on both slow and fast scales. Fast-scale bifurcations cannot be predicted by conventional averaged models, because of the nature of high-frequency and chaotic dynamics [35]. However, we demonstrate the practical control examples of the studied system, for which the conventional method cannot accurately identify slow scale instabilities. To this end, we compare the proposed method with the conventional averaging-based method and discuss the potential advantages of our method. Furthermore, the eigenvalues are utilized to analyze the sensitivity and the robustness of the system's state to parameter variations [41]. The proposed model is advantageous over the conventional methods because: 1) It is not based on the time-series, and hence, the exponential terms are removed. Consequently, the method can be generalized to multi-unit microgrids. 2) The possible transition of the switching command in one switching period is taken into the system model using an additional variable, called a "virtual duty cycle". 3) Stability pattern of the system is constructed using the discrete-time eigenvalues, which can predict the accurate stability margin of the system with different controllers.

Finally, an active stabilizer is applied to the studied system to improve the asymptotic stability of the system. The stabilizer is used to damp the voltage oscillations associated with the low damped LC filter. Fig. 1 (a) shows a typical DC distributed power architecture that is applicable to onboard energy systems for electric transportation [21]. The source-connected converter provides a regulated DC voltage on the distribution bus, and the load converters transfer the DC bus voltage to tightly regulated power, which is desired for electric actuators. An LC filter is also added to the point of load converter. This input filter is used to reject the current and voltage harmonics and to limit electromagnetic interference (EMI) [18]. Such filters are usually poorly damped for reducing losses as well as optimizing size/weight and cost of the total system. A basic model for the stability analysis of DC distribution systems is shown in Fig. 1 (b), comprising of the source and the load subsystems, which is regarded as a generic system configuration. In such a system, from the stability point of view, the load converters can be represented by an instantaneous CPL.
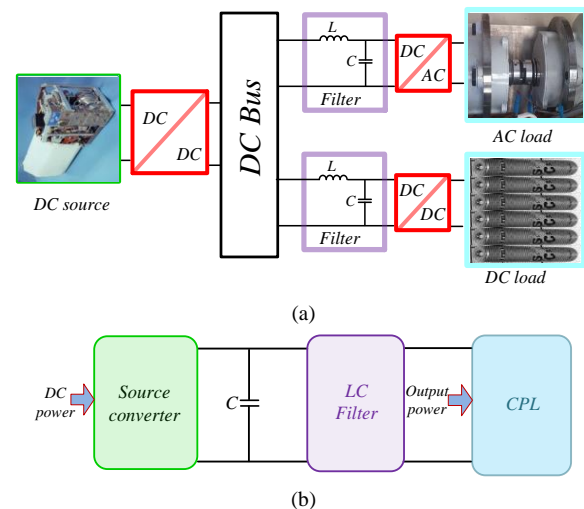

Fig. 1. (a) Schematic of the DC distributed system, (b) Basic model for stability studies.

To deal with the destabilizing effect of low damped DC systems, several techniques have been proposed such as passive damping, virtual capacitor and resistor, and active stabilization [42-46]. Passive methods are not an optimal solution for the on-board electrification, as these techniques increase the size of the system with additional passive components [42, 43]. Linear and nonlinear active stabilization methods are reported in previous research [44-46]. All of these stabilizers are based on the load-side approach, in which the stabilizing commands are applied to the reference power of the load converters.

In this paper, the stabilizer is implemented on the source converter. This method is advantageous over the load-side techniques, because the performance of the stabilizer is not affected by the load controllers. Unlike the centralized approach, with this scheme, the stabilizer does not need additional data. Moreover, this method does not change or modify the control structure, and thus, it can be added as a simple stabilizing block to different types of controllers (i.e. linear or nonlinear). The performance of the stabilizing system is investigated theoretically and experimentally.

The rest of the paper is organized as follows: the studied system and the controller are presented in Section II. The proposed discrete-time model is described in Section III, in which the Jacobian matrix of the system is achieved with minimal calculation by using an intermediary variable. In Section IV, the stability of the system is analyzed, and slow scale and fast scale phenomena are identified. In Section V, the stability analysis of the system is validated experimentally; the experimental results and time domain simulations are put side by side to show the effectiveness of the proposed system analysis.

II. SYSTEM REPRESENTATION AND CONTROLLER

The studied system is presented in this section, including the physical system and the controller. In subsection II.A, the system model is introduced. The controller and stabilizer are presented in II.B.

A. System Model

An electric diagram of the studied system, as a basic system model for the stability analysis, is shown in Fig. 2. The CPL is connected to the DC grid through an input filter. The source converter is a PWM buck DC-DC converter. L and r_L are the series inductance and the resistance of the source converter, respectively. C is the DC bus capacitance. The parameters r_f, C_f, and L_f are the resistance, capacitance, and inductance of the input filter, respectively. The DC source provides the DC voltage V_e. The system model is established in the state-space form.
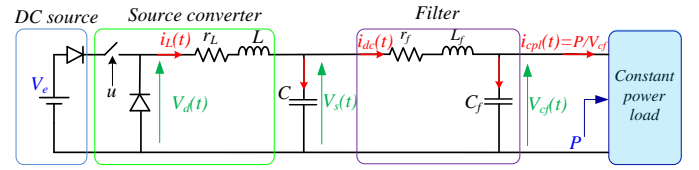

Fig. 2. Schematic of the studied dc power system.

Four physical state variables describe the physical components such as the inductor current i_L, the DC bus voltage V_s, the DC current i_{dc} and the filter voltage V_{cf}. Here, u is the switching command of the source converter. For the stability analysis, the load converter is modeled as a CPL, in which variations in the load current i_{cpl} are associated with variations in the filter voltage V_{cf} in a constant power $(i_{cpl} = \frac{P}{V_{cf}})$. Consequently, the system model has intrinsic nonlinearity because of the load profile of the CPL. In fact, an instantaneous CPL can represent several load converters connected in parallel to the point of load. In this case, the load converters are supposed to be much faster than the source converter. The system model is then described by the state equations:

$$\begin{cases} \dfrac{di_L}{dt} = \dfrac{1}{L}(uV_e - V_s - r_L i_L) \\ \dfrac{dV_s}{dt} = \dfrac{1}{C}(i_L - i_{dc}) \end{cases} \tag{1}$$

$$\begin{cases} \dfrac{di_{dc}}{dt} = \dfrac{1}{L_f}(V_s - V_{cf} - r_f i_{dc}) \\ \dfrac{dV_{cf}}{dt} = \dfrac{1}{C_f}\left(i_{dc} - \dfrac{P}{V_{cf}}\right) \end{cases} \tag{2}$$

B. Control System

Fig. 3 shows the block diagram of the control system, which comprises a voltage control loop and a current control loop. The voltage controller uses a linear proportional-integral (PI) compensator. The current controller is established based on the digital pulse width modulation, and the control law results from the equivalent control approach [47-49]. Digital control variables are considered, since the experimental setup is based on a digital controller. The control variables are thus sampled by a rate of the switching frequency ($T = \frac{1}{f_s}$, f_s: switching frequency), and are used in the controller. The measured and sampled values of the DC current (i_{dc}), output voltage (V_s), and inductor current (i_L) are presented as i_{dcmes}, V_{smes} and i_{Lmes}, respectively.
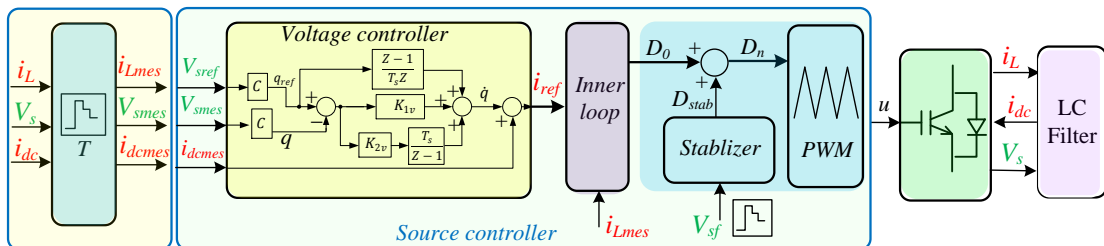

Fig. 3. Block diagram of the control system.

1) Voltage controller

The voltage controller provides a reference current for the inner-loop control. The controller regulates the dc bus voltage by controlling the electric charge in the dc bus capacitor (C). Here, the electric charge has the same dynamics as the voltage, and its derivative is directly related to a current. Therefore, the control law is defined by charge regulation in a digital form, which is presented as a block diagram in Fig. 3, in which the derivative of the electric charge results from a classical PI compensator. In this schematic, $q(t) = C.V_{smes}$, where q is the electric charge, and $q_{ref}(t) = C.V_{sref}$, where q_{ref} is the reference charge.

The control parameters K_{pv} and K_{iv} are the proportional gain and the integral gain of the voltage controller, respectively, and determine the poles of the closed-loop system. These parameters are defined by $K_{pv} = 2\xi\omega_n$ and $K_{iv} = \omega_n^2$, where, ω_n is the desired cut-off frequency and ξ is the damping factor. The reference current i_{ref} thus corresponds to the derivative of the electric charge, and results in (3).

$$
\begin{aligned}
i_{ref} &= \dot{q}(t) + i_{dcmes} \\
\rightarrow i_{ref} &= \dot{q}_{ref}(t) - K_{pv}\left(q(t) - q_{ref}(t)\right) \\
&\quad - K_{iv}\int_0^t \left(q(t) - q_{ref}(t)\right)(\tau)d\tau \\
&\quad + i_{dcmes}
\end{aligned}
\tag{3}
$$

2) Current controller

The current controller regulates the inductor current using a control law defined by function S as given in (4).

$$
\begin{aligned}
S(t) &= i_{Lmes}(t) - i_{ref}(t) \\
&\quad + K_x\int_0^t \left(i_{Lmes}(t) - i_{ref}(t)\right)(\tau)d\tau
\end{aligned}
\tag{4}
$$

where K_x corresponds to the current control bandwidth. This coefficient enables the dynamic response of the controller to be tuned. Then, if the reaching condition $\dot{S} = -\lambda S$ is enforced, the control law including the current error and an integral term is derived. The equation to calculate the control coefficients is detailed in [50]. By applying the resulting control law, the duty cycle of the source converter D_0 results from the system equation, as indicated in (5).

$$
\begin{aligned}
D_0 = \frac{1}{V_e}\Big(&V_{smes} + r_L i_{Lmes} \\
&+ L\Big[(i_{ref} - i_{Lmes})(K_x + \lambda) \\
&- K_x\lambda\int\Big(i_{Lmes}(t) \\
&- i_{ref}(t)\Big)(\tau)\,d\tau\Big]\Big)
\end{aligned}
\tag{5}
$$

3) Stabilizer

To increase stability margin of the system, an additional control command is added to the controller, as a stabilizer. This allows a higher amount of power to be supplied by the source into the DC grid. The stabilizer is implemented with a simple structure: using a proportional compensator followed by a low-pass filter. This filter allows preserving the system dynamics at low frequencies and rejects measurement noise.

An additional duty cycle is produced by the stabilizer, to be added to the main duty cycle. By this approach, the stabilization block could be added to different types of controllers. The stabilization block is shown in Fig. 3, where V_{sf} results from the low-pass filter as follows:

$$
\frac{dV_{sf}}{dt} = \omega_{sf}\left(V_{s,mes} - V_{sf}\right)
\tag{6}
$$

Here, ω_{sf} is an angular frequency corresponding to the voltage oscillations. By applying the stabilization signal, the modified duty cycle D_n results in (7).

$$
D_{stab} = -\frac{1}{V_e}K_{stab}\left(V_{smes} - V_{sf}\right), \; D_n = D_0 + D_{stab}
\tag{7}
$$

In this equation, K_{stab} is the stabilizer's gain, which is chosen with respect to the dynamic performance of the system. The switching signal (u) is then generated through a PWM.

III. PROPOSED DISCRETE TIME MODELLING

In this section, a nonlinear discrete-time model will be obtained. In the proposed discrete-time modeling, two types of state-space representation are considered: continuous representation and sampled representation. The state variables are then divided into two state vectors: continuous variables and sampled variables. The continuous variables are used to describe the physical characteristics of the system, which is detailed in III.A. The sampled vector is defined according to the digital control variables, which are used to calculate the duty cycle, presented in III.B. The digital variables are updated once per switching period (T) and the control variables are sampled and synchronized with the PWM carrier. Consequently, the duty cycle D_n is updated once per switching period for a pulse-width modulation. The state-space model of the system is then completely discretized with the proposed discretization technique in III.C. At this stage, the sampling period (T) is discretized into small sequences, called the discretization period T_e. The Jacobian matrix of the system is calculated in III.D.

A. Physical System Representation

The state vector of the system consists of three sub-vectors: the continuous vector X_c, the control vector X_d and the measurement vector X_{mes}, defined as follows:

$$
X = [X_c^T \; ; \; X_d^T \; ; \; X_{mes}^T]_{10\times1}
\tag{8}
$$

In this definition, X_c contains the physical variables, whereas X_d and X_{mes} are comprised of the sampled variables. Indeed, all the sampled variables are calculated from the continuous variables, and thus, the continuous state-space form is the basis of the discretization. For the continuous form, the state-space equation is formed as indicated in (9), in which c refers to continuous mode.

$$
\dot{X}_c(t) = A_c \cdot X_c(t) + B_c[X_c(t)] \cdot u + N_c[X_c(t)]
\tag{9}
$$

where A_c, B_c, and N_c are the state matrices of the system. The vector of the physical variables $X_c \in \mathbb{R}^4$ is defined as follows:

$$[X_c] = \begin{bmatrix} X_1 \\ X_2 \\ X_3 \\ X_4 \end{bmatrix} = \begin{bmatrix} i_L \\ V_s \\ i_{dc} \\ V_{cf} \end{bmatrix}_{4\times1} \tag{10}$$

Using the system model, the state matrices A_c, B_c and N_c are obtained in (11).

$$A_c = \begin{pmatrix} \frac{-r_L}{L} & \frac{-1}{L} & 0 & 0 \\ \frac{1}{C} & 0 & \frac{-1}{C} & 0 \\ 0 & \frac{1}{L_f} & \frac{-r_f}{L_f} & \frac{-1}{L_f} \\ 0 & 0 & \frac{1}{C_f} & 0 \end{pmatrix}, B_c = \begin{pmatrix} \frac{V_e}{L} \\ 0 \\ 0 \\ 0 \end{pmatrix},$$

$$N_c = \begin{pmatrix} 0 \\ 0 \\ 0 \\ P \\ -\frac{P}{C_f \cdot X_4} \end{pmatrix} \tag{11}$$

The linear terms are regrouped in the matrices A_c and B_c, whereas N_c contains the nonlinearity of the system model.

B. Representation of Sampled Variables

The sampled variables include the measured variables and the control variables ($[X_d^t \; ; \; X_{mes}^t]_{6\times1}$), and are updated once per sampling period T. It should be noted that T is equal to the switching period, and is different from the discretization period T_e. The measured variables are the system variables, which are measured and sampled to calculate the control command. The state-space form of the control variables is defined in (12), where d refers to the digital form. In this equation, X_d and X_{mes} are digital vectors representing control variables and measured variables, respectively.

$$\dot{X}_{d(n)} = \frac{X_{d(n+1)} - X_{d(n)}}{T} \tag{12}$$
$$= A_d \cdot X_{d(n)} + M_d + E_n \cdot X_{mes(n)}$$

Matrix A_d is the digital state matrix, applied to the control state-variables, M_d is the matrix of constant parameters, and E_n is the control matrix applied on the measured variables. The control state vector $X_{d(n)} \epsilon \mathbb{R}^3$ is defined as follows:

$$[X_d] = \begin{bmatrix} V_{sf} \\ int(i) \\ int(q) \end{bmatrix}_{3\times1} \tag{13}$$

where $int(q)$ is the discrete-time integral of the electric charge error ($q(t) - q_{ref}(t)$), and $int(i)$ is the discrete-time integral of the inductor current error ($i_{Lmes}(t) - i_{ref}(t)$). $X_{mes} \epsilon \mathbb{R}^3$ contains the measured values of the variables:

$$[X_{mes}] = \begin{bmatrix} i_{Lmes} \\ V_{smes} \\ i_{dcmes} \end{bmatrix}_{3\times1} \tag{14}$$

Using the control equations, the state space form of X_d from (12) can then be expressed as:

$$\dot{X}_{d(n)} =$$
$$\begin{bmatrix} \omega_f(V_{smes} - V_{sf}) \\ i_{Lmes} + K_{1v}(C \cdot V_{smes} - C \cdot V_{sref}) + K_{2v} \cdot int(q) - i_{dcmes} \\ C \cdot V_{smes} - C \cdot V_{sref} \end{bmatrix} \tag{15}$$

Finally, (15) can be used to deduce the digital matrices A_d, M_d and E_n in (16).

$$A_d = \begin{pmatrix} -\omega_f & 0 & 0 \\ 0 & 0 & K_{2v} \\ 0 & 0 & 0 \end{pmatrix},$$

$$M_d = \begin{pmatrix} 0 \\ -K_{1v} \cdot C \cdot V_{sref} \\ -C \cdot V_{sref} \end{pmatrix}, E_n = \begin{pmatrix} 0 & \omega_f & 0 \\ 1 & K_{1v} \cdot C & -1 \\ 0 & C & 0 \end{pmatrix} \tag{16}$$

It should be noted that the digital derivative of the control variables will not result from the Euler approximation. Instead, it will be calculated at the end of each period.

C. Discretization of the System Model

The objective of this section is to establish a relationship between the state vector X_n at instant nT and the vector X_{n+1} at instant $(n+1)T$, without linearization. Consequently, a discrete-time Poincare map can be defined by $X_{n+1} = F(X_n, nT)$. The switching command u is generated with a symmetric PWM. The PWM period T is then divided into N_p small sequences, as illustrated in Fig. 4. ($T_e = \frac{T}{N_p}$). All the continuous state variables are sampled and updated N_p times per switching period. The rate of N_p is called the discretization rate, and the resulting period T_e is called the discretization period, which is used as a sequence in the Euler approximation.

Then, using the Euler approximation, the state-space form of the continuous sub-model in (9) results in:

$$\frac{X_{c((k+1)T_e)} - X_{c(k\,T_e)}}{T_e} =$$
$$A_c \cdot X_{c(k\,T_e)} + B_c[X_{c(k\,T_e)}] \cdot u + M_c + N_c[X_{c(k\,T_e)}] \tag{17}$$

where k is a counter for the discretization sequences during each switching period ($k = 1: N_p$).

In each switching period T, the switching command u changes from one to zero during one discretization period (T_e), and changes back to one during another sequence (see Fig. 4.). It should be noted that every sequence is equal to T_e. In this method, the instant at which the change of u is assumed to be unknown. Thus, the performance of the model does not depend on the instant at which the command changes, and hence, the model can be applied to either digital controllers or analog controllers.
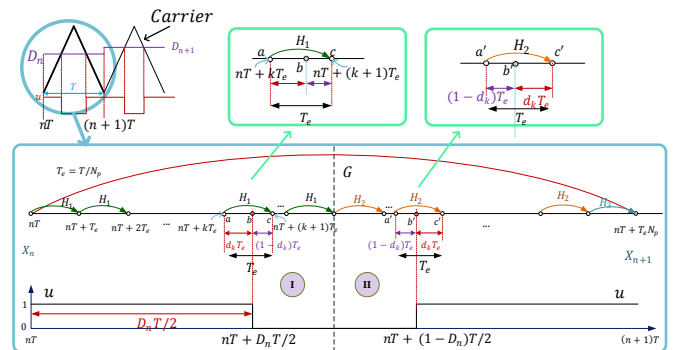

Fig. 4. Discretization in each switching period of the symmetric PWM.

An additional nonlinear variable is then added to the state-space model, called a virtual duty cycle d_k, to take into account the change of the command (u). This variable is later used in the Jacobian calculation. The virtual duty cycle d_k determines the instant at which u changes during a discretization period T_e (see Fig. 4). Using d_k, each discretization period, such as the interval $[a, c]$, can be divided into two sub-intervals, as indicated in Fig. 4. The duration of the first sub-interval is equal to $d_k T_e$. The variable d_k is defined by an intermediary variable d_k^*. Then, d_k is obtained by the saturation of the variable d_k^* between $[0,1]$, using function Sat defined as follows:

$$d_k = Sat(d_k^*) = (1 - d_k^*)\left(0.5 + \frac{atan(a(d_k^* - 1))}{\pi}\right)$$
$$+ d_k^*\left(0.5 + \frac{atan(ad_k^*)}{\pi}\right) \qquad (18)$$

As mentioned before, d_k will be used to calculate the Jacobian matrix. The function $sat(d_k^*)$ is then defined as continuous and differentiable at all points, and also the dynamic properties of the system are preserved [11]. Here, a standard saturation is not preferred as its derivative is discontinuous at the singular points. Therefore, we tuned a nonlinear saturation function to fit as accurately as possible into the singularities of the original function (d_k^*).

The intermediary variable d_k^* is defined in two sections. Consequently, two different discrete functions are defined: H_1 and H_2, for $k < \frac{N_p}{2}$, and $k \geq \frac{N_p}{2}$, respectively (see Fig. 4). The function H_3 is also defined to update the digital variables. The discrete functions are established by defining d_k^* as follows:

1) For $k < \frac{N_p}{2}$ ($t < nT + \frac{T}{2}$), u changes from 1 to 0, and d_k^* is defined by (19).

$$d_k^* = \frac{D_n \frac{T}{2} - k\, T_e}{T_e} \qquad (19)$$

At this stage, a recurring function is needed to map the state variables at time $n\, T_s + (k + 1)T_e$ to those at the previous instant $n\, T_s + k\, T_e$. For the sake of clarity, an interval $[a, c]$ is considered, with two sub-intervals $[a, b]$, and $[b, c]$, to obtain the recurring function. In the first sub-interval $[a, b]$, the time variable changes from $n\, T + k\, T_e$ to $n\, T + (k + d_k)T_e$. According to Fig. 4, the Euler approximation can then be rewritten as follows:

$$\frac{X_c[b] - X_c[a]}{b - a} = A_c \cdot X_c[a] + B_c \cdot \underset{1}{\underbrace{u}} + M_c + N_c[a] \qquad (20)$$

where $b - a = d_k\, T_e$, then:

$$X_c[b] = X_c[a] + d_k T_e \cdot A_c \cdot X_c[a] + d_k T_e \cdot B_c$$
$$+ d_k T_e \cdot N_c[a] + d_k T_e \cdot M_c \qquad (21)$$

In the second subinterval $[b, c]$, the time variable changes from $n\, T + (k + d_k)T_e$ to $nT + (k+1)T_e$. According to Fig. 4, the Euler approximation is formulated as follows:

$$\frac{X_c[c] - X_c[b]}{c - b} = A_c \cdot X_c[b] + B_c \cdot \underset{0}{\underbrace{u}} + M_c + N_c[b] \qquad (22)$$

where $b - a = d_k\, T_e$, then:

$$c - b = (1 - d_k)T_e \Rightarrow X_c[c]$$
$$= X_c[b] + (1 - d_k)T_e \cdot A_c$$
$$\cdot X_c[b] + (1 - d_k)T_e \cdot N_c[b] \qquad (23)$$
$$+ (1 - d_k)T_e \cdot M_c$$

The two equations (21) and (23) enable the discrete function H_1 (see Fig. 4), to be established within the interval $[nT, nT + \frac{T}{2}]$ as follows:

$$X_{(k+1)T_e} = H_1\big(X_{k\, T_e}, d_k\big)$$
$$= \big(A \cdot X_{(k+d_k)T_e} + M$$
$$+ N[X_{(k+d_k)T_e}]\big)(1 - d_k)T_e \qquad (24)$$
$$+ \big(A \cdot X_{k\, T_e} + B[X_{k\, T_e}] + M$$
$$+ N[X_{k\, T_e}]\big) \cdot d_k T_e + X_{k\, T_e}$$

2) For $k \geq \frac{N_p}{2}$, u changes from 0 to 1 during the interval $[a', c']$. The intermediary variable d_k^* is then calculated in each discretizing period T_e as follows:

$$d_k^* = \frac{D_n \frac{T}{2} - T + (k + 1)T_e}{T_e} \qquad (25)$$

The duty cycle verifies $d_k = Sat(d_k^*)$, and the Euler equation is calculated again in two sub-interval for each sequence and the discrete function H_2 is defined:

$$X_{(k+1)T_e} = H_2\big(X_{k\, T_e}, d_k\big); \; for\; k > \frac{T}{2T_e} \qquad (26)$$

It should be noted that the functions H_1 and H_2 are a function of $X_{k\, T_e}$ and d_k. However, in each step, d_k can be derived from (19) and (25) with the saturation function of (18). Therefore, the discrete function relate $X_{(k+1)T_e}$ with an implicit function to $X_{k\, T_e}$. The recurring function is then established for all points during the switching period. In the last sequence of each switching period ($k = N_p$), the function H_3 is defined to update the two digital vectors at the instant $(n + 1)T$. Hence, H_3 is called the update function. It then gives the new digital vector $[X_d^t\; X_{mes}^t]_{(n+1)T}$, and the new state vector then results in:

$$X_{n+1} = H_3\big(X_{k\, T_e}, X_{nT}\big) \qquad (27)$$

Finally, the measured vector X_{mes} is calculated using the continuous vector at the end of the switching period:

$$X_{mes(n+1)T} = \big[X_{(k+1)T_e}(1), X_{(k+1)T_e}(2), X_{(k+1)T_e}(3)\big]^T \qquad (28)$$

We would like to emphasize that the update function H_3 is applied to the digital vector only in the last sequence of each period, and during the rest of the period these variables are constant. The proposed discrete model is summarized, for one switching period, in (29). Here, H_1, H_2, and H_3 are predefined discrete functions.

$$H_1: \begin{bmatrix} X_{c(kT_e)} \\ X_{d(n)} \\ X_{mes(n)} \end{bmatrix} \underbrace{\quad}_{X_{n,k}} \xrightarrow{u=1} \begin{bmatrix} X_{c(k+d_k)T_e} \\ X_{d(n)} \\ X_{mes(n)} \end{bmatrix} \underbrace{\quad}_{X_{n,k+d_k}} \xrightarrow{u=0} \begin{bmatrix} X_{c(k+1)T_e} \\ X_{d(n)} \\ X_{mes(n)} \end{bmatrix} \underbrace{\quad}_{X_{n,k+1}}$$

$$H_2: \begin{bmatrix} X_{c(kT_e)} \\ X_{d(n)} \\ X_{mes(n)} \end{bmatrix} \underbrace{\quad}_{X_{n,k}} \xrightarrow{u=0} \begin{bmatrix} X_{c(k+d_k)T_e} \\ X_{d(n)} \\ X_{mes(n)} \end{bmatrix} \underbrace{\quad}_{X_{n,k+d_k}} \xrightarrow{u=1} \begin{bmatrix} X_{c(k+1)T_e} \\ X_{d(n)} \\ X_{mes(n)} \end{bmatrix} \underbrace{\quad}_{X_{n,k+1}} \quad (29)$$

$$H_3: \begin{bmatrix} X_{c(n,k_2 T_e)} \\ X_{d(n)} \\ X_{mes(n)} \end{bmatrix} \underbrace{\quad}_{X_{n,k}} \xrightarrow{u=1} \begin{bmatrix} X_{c(n+1)} \\ X_{d(n+1)} \\ X_{mes(n+1)} \end{bmatrix} \underbrace{\quad}_{X_{n+1}}$$

Using the presented discretization method, a system function G (see Fig. 4) composed of the discrete functions can be defined. The system function G^{oN_p} is calculated and updated N_p times in each period. By introducing $k_1 = \frac{N_p}{2}$, and $k_2 = N_p - 1$, G^{oN_p} can be expressed as follows:

$$X_{(n+1)T} = G^{oN_p}(X_{nT})$$
$$= H_{3,N_p} \circ H_{2,k_2} \circ \cdots \circ H_{2,k_1+1} \circ H_{1,k_1} \quad (30)$$
$$\circ \cdots \circ H_{1,1}(X_{nT})$$

where $H_{i,k}$ is the discrete function H_i calculated at instant $nT + kT_e$. The resulting system function contains the system dynamics.

PWM time delay

In digital controllers, usually a time delay is introduced by the PWM. In this case, the duty cycle will be updated after a delay which depends on the hardware. The time delay can be considered in the proposed model by modifying the digital representation. For the case in which one sample delay (T) is introduced, X_{nT} will be replaced by $X_{(n-1)T}$ in the definition of D_n.

D. Calculation of Jacobian Matrix

The Jacobian matrix of the complete system can be calculated from the resulting system model [41]. For the time-domain expression, a time variable $nT + kT_e$ is introduced comprised of the switching period and the discretization sequence. The new space-vector $X_k \epsilon \mathbb{R}^{11}$ is defined as follows:

$$X_k = [X_c^t ; \; X_d^t ; \; X_{mes}^t ; n\,T + k\,T_e]_{11\times1} \quad (31)$$

As mentioned before, H_i is a function of X_k and d_k, while d_k relates to the intermediary variable d_k^*. Partial differential equations (PDEs) can then be established for H_i with the variation of d_k^*. Following a small perturbation around an equilibrium point (X_0, d_{k0}), a first order approximation of H_i results in:

$$H_i(X_0, d_{k0} + dd_k) = H_i(X_0, d_{k0}) + dH_i(X_0, d_{k0})$$
$$\text{where: } dH_i(X_0, d_{k0}) = \left(\frac{\partial H_i}{\partial x}\right)_{(X_0, d_{k0})} dX_k + $$
$$\left(\frac{\partial H_i}{\partial d_k}\right)_{(X_0, d_{k0})} dd_k \quad (32)$$

In this stage, partial derivative of d_k (dd_k) is to be defined using the variable d_k^*. For this objective, a control variable is introduced as a function of the index k and the variable d_k^* in:

$$s_k = d_k^* - \left(D_n \frac{T}{2} - k\,T_e\right)/T_e \quad (33)$$

Using the control variable s_k being equal to zero, a partial derivative of d_k^* is defined as follows:

$$\frac{\partial s_k}{\partial X_k} dX_k + \frac{\partial s_k}{\partial d_k} dd_k^* = 0 \Rightarrow dd_k^*$$
$$= -\left(\frac{\partial s_k}{\partial d_k}\right)^{-1}\left(\frac{\partial s_k}{\partial X}\right) dX_k \quad (34)$$

With the saturation function introduced in (18) and the relation (34), we obtain dd_k by:

$$dd_k = \frac{\partial sat(d_k^*)}{\partial d_k^*} dd_k^* \Rightarrow$$
$$dd_k = -\frac{\partial sat(d_k^*)}{\partial d_k^*}\left(\frac{\partial s_k}{\partial d_k}\right)^{-1}\left(\frac{\partial s_k}{\partial X}\right) dX_k \quad (35)$$

By replacing (35) in (32), the PDEs can then be expressed as follows:

$$dH_i(X_0, d_{k0})$$
$$= \left(\frac{\partial H_i}{\partial X_k}\right) dX_k$$
$$-\left(\frac{\partial H_i}{\partial d_k}\right)\frac{\partial sat(d_k^*)}{\partial d_k^*}\left(\frac{\partial s_k}{\partial d_k}\right)^{-1}\left(\frac{\partial s_k}{\partial X_k}\right) dX_k \quad (36)$$

The Jacobian matrix of the complete system is then calculated using the three sub-systems H_i, given before. The arguments of the Jacobian of the sub-system H_i are obtain by:

$$J_{H_i,k} = \frac{\partial H_i}{\partial X_k} - \frac{\partial H_i}{\partial d_k}\frac{\partial sat(d_k^*)}{\partial d_k^*}\left(\frac{\partial s_k}{\partial d_k}\right)^{-1}\left(\frac{\partial s_k}{\partial X_k}\right) \quad (37)$$

Finally, the Jacobian matrix of the composed system function G, named J_G, can be calculated as follows:

$$J_G = J_{H_3,N_p} \times J_{H_2,k_2} \times \cdots \times J_{H_2,k_1+1} \times J_{H_1,k_1} \times \cdots \times J_{H_1,1} \quad (38)$$

where $J_{H_i,k}$ is the Jacobian matrix of the function H_i calculated at instant $nT + kT_e$. By calculating J_G, the eigenvalues of the complete system are obtained. The composed function G contains the nonlinear system dynamics.

The asymptotic stability of the system can be studied using the eigenvalues of the Jacobian matrix at an equilibrium point. Eigenvalues of the discrete-time system are also called Floquet multipliers [40]. In the next section, Floquet multipliers are used to identify instabilities in the system.

IV. STABILITY ANALYSIS USING THE PROPOSED MODEL

The stability of the studied system can be analyzed by the proposed method: the system eigenvalues are calculated from the Jacobian matrices of the system, and system bifurcations are studied using a discrete Poincare formulation. The dynamic behavior of the system can then be studied using bifurcation diagrams, and the asymptotic stability of the system is investigated using the eigenvalues. A background of the system analysis is given in IV. A. The stability analysis and dynamic performance evaluation of the studied system are then performed with the proposed method, in IV. B. Different case studies have been performed with different filter parameters and control parameters. In each case, the stable and unstable operating points are identified using the pattern of the system's eigenvalues. The performance of the stabilizer is evaluated in IV. C; the robustness of the stabilizer to the parameter variations is also studied in this subsection. The proposed method is compared with the conventional method in IV. D.

A. Description of the System Analysis

The asymptotic stability of the system can be studied using the eigenvalues of the system model at the equilibrium point. Eigenvalues of the discrete-time system are also called Floquet multipliers. In the discrete-time systems, the loss of stability of the periodic solution corresponds to the unit circle crossed by one or more eigenvalues of the Jacobian matrix. The system is stable if all the multipliers have a magnitude of less than 1. In the complex plane, the classification of bifurcations depends on where the eigenvalues cross the unit circle. In this illustration, as a bifurcation parameter changes, the eigenvalues move in the complex plane. If an eigenvalue moves outside the unit circle, three possible bifurcations can occur, namely, flip (or period-doubling), Neimark-Sacker (or Hopf bifurcation), or Saddle-node bifurcation [40, 41]. The first two types of the instabilities, Neimark and flip, are common in power electronic systems [9]. When a complex conjugate pair of eigenvalues simultaneously crosses the unit circle, a Neimark-Sacker bifurcation is obtained, which results in a periodic limit cycle or a quasi-periodic solution. A flip bifurcation type occurs if at least one eigenvalue crosses the unit circle on the negative real axis [51].

The nature of instabilities is also studied with bifurcation diagrams. The term "bifurcation" is used to describe the loss of stability at a given operating point called the "bifurcation point" [40]. Beyond this point, the system variables bifurcate into unstable states, and thus, it is important to detect the bifurcation point to prevent catastrophic consequences. Bifurcation diagrams have been used in qualitative studies examining how the characteristics of the system change as a function of a parameter in the system called a "bifurcation parameter", such as a passive element or a control parameter [32]. Here, the power absorbed by CPL (P) is considered to be the bifurcation parameter. The system loses stability at a bifurcation point, which is associated with a specific power. The diagrams are plotted using sufficient data sets of the state variables resulting from the discrete-time model of the system. This is repeated for the different values of the bifurcation parameter (P). Each bifurcation diagram illustrates the system dynamics associated with a specific system configuration.

B. Stability Analysis of the Studied System With the Proposed Method

In this study, two cases with different system parameters, and thus different dynamic behaviors, are investigated. The values of the filter parameters for the two cases are given in Table I. Parameters of the outer-loop control such as K_{pv} and K_{iv} are also listed in Table I. These control parameters are designed such that the bandwidth of the voltage controller is sufficiently lower than that of the current controller ($\omega_n < \frac{K_{x,min}}{10}$). If the minimum bandwidth of the current controller is considered to be $K_{x,min} = 1000$, the bandwidth of the outer-loop is set to $\omega_n = 70 \, rad \cdot s^{-1}$. The outer-loop control is fixed for all of the case studies. In this section, the bandwidth of the current controller is set to $K_x = 2000$, and the stabilizer's gain $K_{stab} = 0$. However, these parameters will be changed during the case studies.

TABLE I
VALUES OF PASSIVE COMPONENTS AND CONTROL PARAMETRS

Parameter	Value	Parameter	Value
L	$2 \, mH$	K_{iv}	98
C	$435 \, \mu F$	K_{pv}	4900
r_L	$0.13 \, \Omega$	$K_{x,min}$	1000
f_s	$10 \, kHz$	λ	1000
V_{sref}	150 V	ω_{sf}	$630 \, rad \cdot s^{-1}$
Filter parameters			
Parameter	Case I		Case II
L_f	$525 \, \mu H$		$120 \, \mu H$
C_f	$38 \, \mu F$		$8.5 \, \mu F$
r_f	$0.16 \, \Omega$		$0.12 \, \Omega$

1) Case I

First, the system model is simulated with the parameters from case I, with the discrete-time model. The bifurcation diagram of the filter voltage $V_{cf}(t)$ and the DC current $i_{dc}(t)$ are presented in Fig. 5, where the CPL power (P) is the bifurcation parameter [41]. The system model is established for each value of P. The bifurcation occurs when the load power is $P = P_0 = 680W$, and this point (P_0) is called critical power. Beyond this point, slow-scale bifurcation occurs, and the dynamics of the system can be described by Neimark–Sacker bifurcation [41]. However, quasi-periodic orbits appear in higher ranges of power. Two different system dynamics are observed from the bifurcation: quasi-periodic orbits (ex: P =800 W) and limit cycles (ex: P =1200 W).

The discrete-time eigenvalues or Floquet multipliers are calculated from the Jacobian matrix of the system, and are indicated in Fig. 6, for different values of P from 100 W to 1000 W. Arrows in Fig. 6 (a) show the trajectories of the eigenvalues as P is increased. The multipliers leave the unit circle when $P > P_0$.

The maximum magnitudes of the eigenvalues are also indicated in Fig. 6 (b): if the eigenvalues cross the horizontal line (magnitude =1), the system loses stability. The critical power or the stability margin, resulting from the pattern of the eigenvalues, is consistent with the bifurcation point calculated from the bifurcation diagram ($P_0 = 680W$). This proves the Jacobian matrix calculation, which is the basis for the stability analysis.
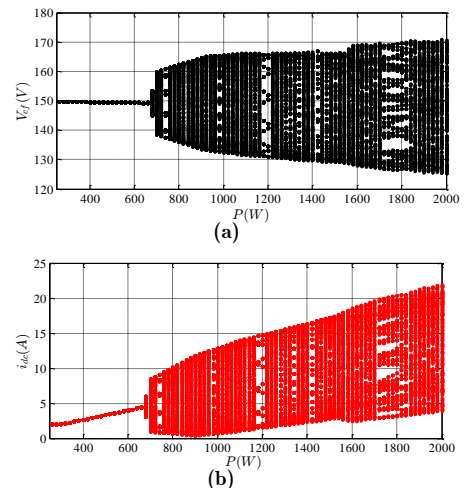

(a)

(b)

Fig. 5. Bifurcation diagrams with changes in CPL power (P) for the parameters case I, and $K_{stab} = 0$: (a) filter voltage V_{cf}; (b) dc current i_{dc}.
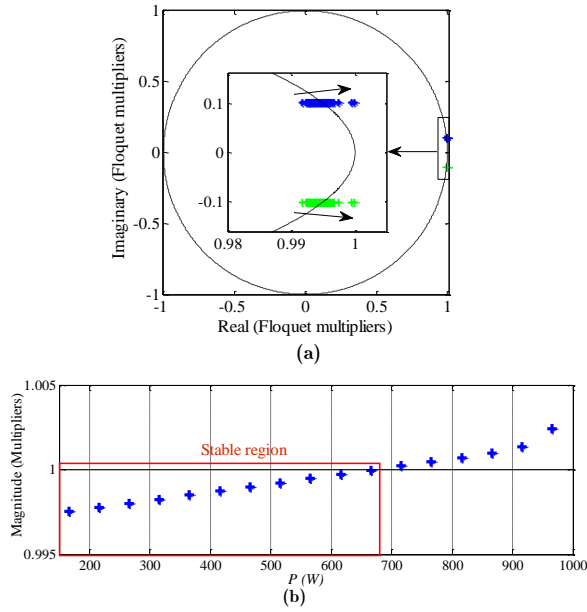
(a)

(b)

Fig. 6. Changes to the eigenvalues with the variation of P in case I, $K_{stab} = 0$: (a) Evolution of multipliers in the unit circle, (b) magnitude of the eigenvalues.

2) Case II

Here, the simulations are repeated with parameters from case II. The bifurcation diagram of the system for both the filter voltage (V_{cf}), and current $i_{dc}(t)$ are indicated in Fig. 7. The critical power P_0 is around 1300 W. At power levels greater than P_0, the nature of the orbit changes, such that the state trajectory describes a double cycle. This phenomenon results in a period-2 or flip bifurcation [51]. Changes to the Floquet multipliers as a function of P is shown in Fig. 8: the eigenvalues leave the unit circle across the real axis (through the point (-1, 0)). The stable period-1 solution is lost and replaced with a period-2 solution. This phenomenon is caused by the fast-scale bifurcation predicted by the diagrams of Fig. 7. Thus, discrete multipliers can be used to identify the dynamics of the system.
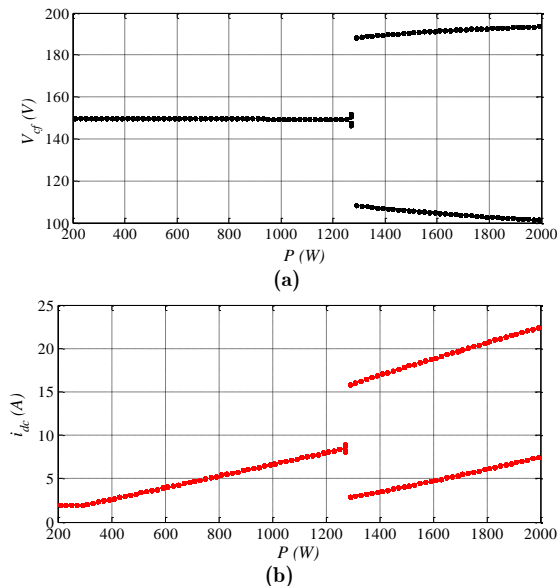

(a)

(b)

Fig. 7. Bifurcation diagrams with the variation of P for the parameters case II, and $K_{stab} = 0$: (a) filter voltage (V_{cf}); (b) dc current i_{dc}.
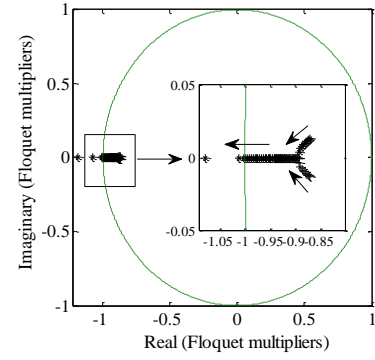

Fig. 8. Evolution of multipliers, with the variation of P, with parameters case II, $K_{stab} = 0$.

C. Stabilization and Robustness Analysis

Here, the stabilizer is also studied using the proposed method. The stabilizer's gain is set to $K_{stab} = 6.3$. This gain is chosen as a sub-optimal value with respect to the dynamic response of the system. Again, Floquet multipliers are calculated for the simulation scenario of the case I, when using the stabilization signal. The magnitudes of the multipliers are presented in Fig. 9, when P varies. It is observed that the critical power is increased to around 1100 W (compared to Fig. 6). It verifies the effectiveness of the stabilizer to extend the stability margin of the system.

The advantage of the discrete-time model, compared to the numerical simulation, is that it provides a quantitative analysis of the stability of the operating point and allows studying the sensitivity of the system's state to the variation of the parameters. For this objective, the filter capacitance (C_f) is changed by $\pm 25\%$. Typically, reducing the capacitance, while keeping the power rating, causes the loss of stability. The stabilization system is tested when changing the C_f, with a constant power of $P = 650\,W$ and the parameters of case I. Multipliers are plotted in Fig. 10, for two cases of without stabilizer ($K_{stab} = 0$), and with stabilizer ($K_{stab} = 6.3$). They leave the unit circle without stabilizer, and remain inside the unit circle only when the stabilization signal is used. This guarantees the stability of the system for a range of parameter changes. The sensitivity analysis is also a step-forward in the control design, since this enables tuning the control parameters such that the system stability is ensured.
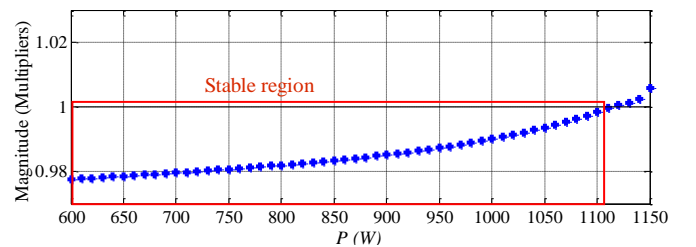

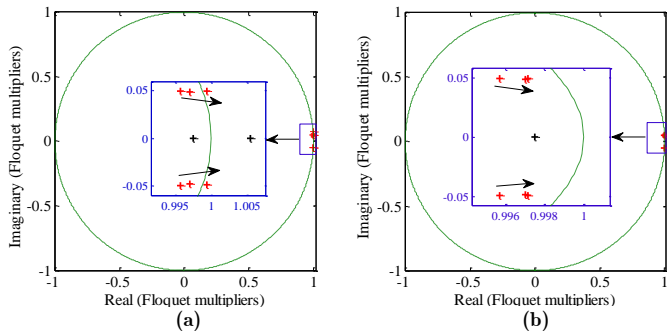Fig. 9. Magnitude of the eigenvalues with the changes in P, with stabilization signal, $K_x = 2000, K_{stab} = 6.3$.

Fig. 10. Evolution of multipliers with the variation of the filter capacitance (C_f) from 50 to 30 µF: (a) without stabilizer, (b) with stabilizer.

D. Comparison With the Averaged Model

Here the proposed model is evaluated and compared with the averaging method, for the simulation scenario case I. The effect of changing the CPL power and the control bandwidth K_x are investigated. Given that the current controller is designed to be much faster than the voltage controller, the dynamics of the system are mainly influenced by the bandwidth of the current controller, which is defined by K_x. First, the stability of the system has been analyzed with the averaged model, and the eigenvalues are calculated when K_x and P change. The stable and unstable operating points are identified and shown with blue circles and red crosses, respectively, in Fig. 11 (a). A model of the system is then constructed again with the proposed discrete-time method, and the results of eigenvalues are indicated in the stability pattern of Fig. 11 (b). It can be observed that, in general, high power can be controlled in the system by increasing the control bandwidth. However, the stability regions identified by the two methods are different. This analysis reveals two critical cases in which the averaged model fails to identify the dynamic properties of the system.

When the control bandwidth is increased ($K_x > 2000$), the averaged model shows that the system loses stability at load powers higher than 700 W, whereas the proposed method here indicates that the system can work for load powers up to $P = 900 \,\text{W}$. Therefore, the conventional method underestimates the critical power and the stability margin of the system. When $K_x \leq 2000$, the averaged model indicates that the system is stable in a larger range of power, whereas the nonlinear analysis indicates that the system may have oscillatory modes. For instance, if $K_x = 1000$, the critical power detected by the proposed method is $P = 380 \,\text{W}$, whereas the averaging method suggests that the maximum power is $P = 580 \,\text{W}$. Therefore, the conventional method substantially overestimates the stability margin in comparison to the proposed method. In fact, the conventional method fails to detect instability.

The nonlinear effect of the switching frequency is neglected in the averaged model; consequently, the fast-scale dynamics of the system are neglected. Moreover, the nonlinear dynamic of the system is exaggerated by the constant power characteristics of the load. Indeed, the fast load dynamic can be represented by an instantanous CPL. It enables the fast-scale changes to propage into the system, and imposes a nonlinear dynamic to the system model.
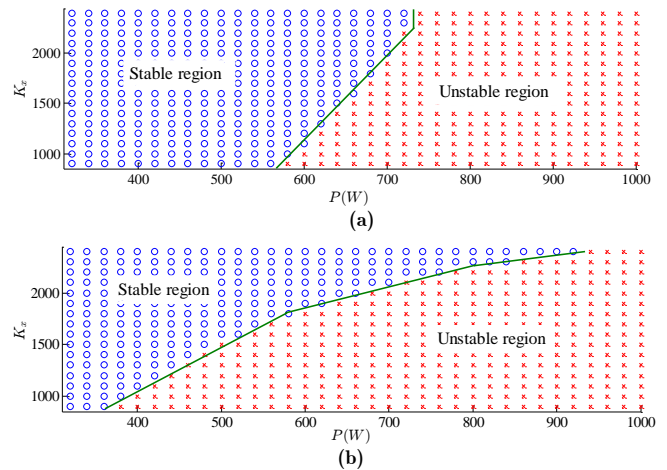

Fig. 11. Stability pattern of the system with change in the control gain and the load power. (a) Results from the conventional averaging method. (b) Results from the proposed discrete-time model.

This produces a degrading effect on the dynamics of the system, which is further intensified by changing the dynamics of the controller, as demonstrated in Fig. 11. In this case, the system model cannot be linearized because of the fast and unpredictable changes in the state of the system. The interaction between the switching effect and the nonlinear dynamics of the load gives rise to instabilities in the system. Therefore, the linearized method based on averaging is no longer accurate. By contrast, the discrete-time method proposed here identifies the instabilities, and is not influenced by the system's dynamics. In section V, these observations are verified experimentally, as well as by time-domain simulations.

V. Experimental Validation

The proposed discrete-time model is validated here using a laboratory test bed. A buck converter supplies the load through an LC filter. The DC input voltage (V_e) is provided by a programmable power supply. The DC source provides an input voltage of 270 V, and the maximum source current is limited to 10 A. The converters are implemented by Semikron insulated-gate bipolar transistors (IGBTs), and are controlled by a dSPACE real-time control card (DS1103). A DC converter is used as the load. The power absorbed by the load converter is supposed to be tightly controlled to simulate accurately fast load dynamics. Therefore, the control bandwidth of the load converter was chosen to be sufficiently higher than that of the source converter. The system's parameters are the same as those in the simulation model.

Different case studies were investigated: the effect of the control bandwidth on the stability of the system is studied in V. A; time-domain simulations are also performed to further support the proposed stability analysis; the dynamic behavior of the stabilizer is then investigated experimentally in V. B. First, the dynamic performance of the controller is investigated, as shown in Fig. 12. The reference power P is changed stepwise from 500 W to 600 W, in a constant voltage ($V_s = 150 \,V$). The current and voltage waveforms indicate the step response of the controller, in which, the overshoot of the current (i_L) is less than 2 A and is within the acceptable range of the current's variations.
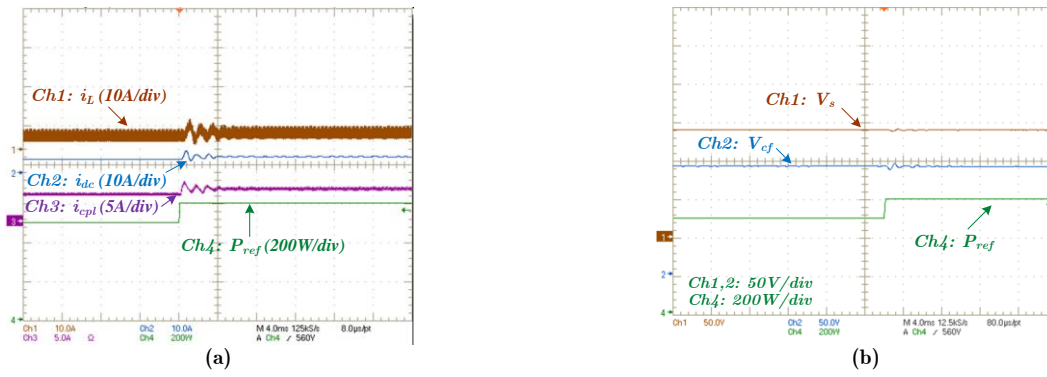
(a)   **(b)**

Fig. 12. Dynamic behavior of the controller, $P = 500 \rightarrow 600W$: (a) currents; (b) voltages.

A. Stability Analysis of the System With Different Values of K_x

To verify the stability analysis in Section IV, laboratory experiments are performed for three different scenarios corresponding to the different control parameters. The results are compared with those of the proposed method in Fig. 11 (b). Moreover, the experimental results and the time domain simulations are put side by side to show the effectiveness of the proposed system analysis. The simulation results are scaled same as the scope display, in order to have a comparison between the time-domain simulations and the experiments.

In the first scenario, the control bandwidth is set to $K_x = 2000$. The CPL power is set to $P = 650\ W$, as a stable operating point, and the experimental results are shown in Fig. 13 (a). The AC input coupling of the oscilloscope is used to filter the DC voltage and to present the voltage oscillations only v_s. The time-domain simulation is also performed for the same scenario, as presented in Fig. 13 (b).

The power is then increased to $P = 700\ W$, which was identified as an unstable operating point by the proposed method in Fig. 11 (b). The experimental waveforms of the currents and voltages of the system are indicated in Fig. 14 (a) and Fig. 15 (a), respectively. The simulation waveforms, for the same scenario, are presented in Fig. 14 (b) and Fig. 15 (b), presenting the system currents and voltages. The limit cycle oscillations are observed from both the experiment and the simulation. These results validate the bifurcation predicted by the bifurcation map in Fig. 5.

In the second scenario, the experiments are repeated with $K_x = 1000$. The experimental and simulation waveforms of the currents and the DC voltage (v_s) are shown in Fig. 16 for $P = 520\ W$, a load power at which the system variables are oscillating. The experimental results, which are indicated in Fig. 16 (a), show the same dynamics as the simulation waveforms, which are presented in Fig. 16 (b). The results of this analysis are consistent with the stability pattern derived from the proposed method in Fig. 11 (b).
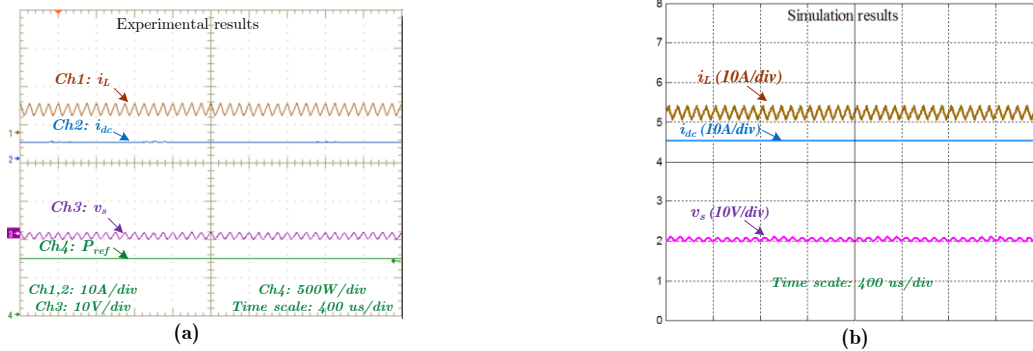

(a)   **(b)**

Fig. 13. Steady-state currents and dc voltage (v_s) for the first scenario ($K_x = 2000$), $P = 650W, K_{stab} = 0$, (a) experiment; (b) simulation.

(a)   **(b)**
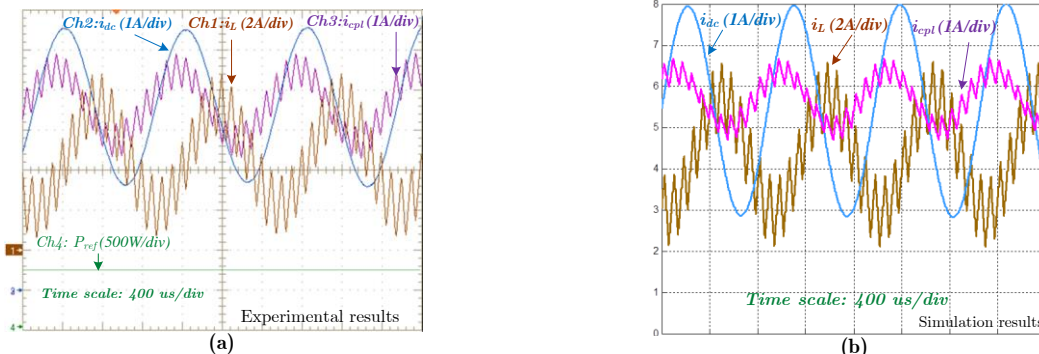
Fig. 14. Steady-state current waveforms for the first scenario ($K_x = 2000$), $P = 700W, K_{stab} = 0$, (a) experiment; (b) simulation.
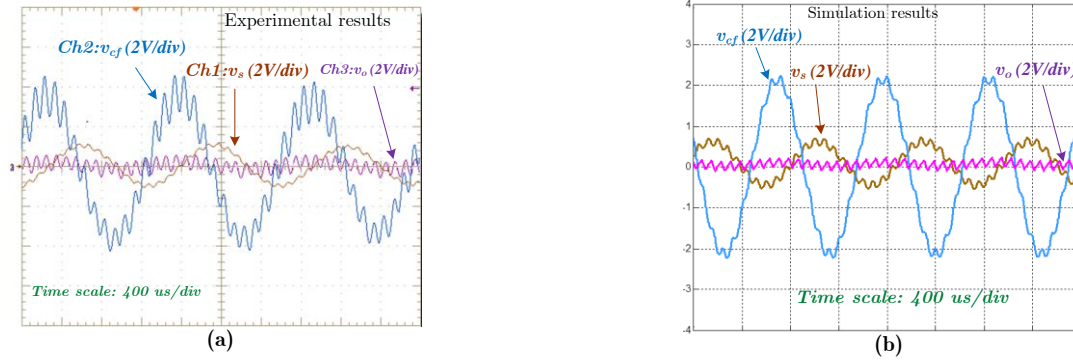
Fig. 15. Steady-state voltage waveforms for the first scenario ($K_x = 2000$), with $P = 700W$, $K_{stab} = 0$, (a) experiment; (b) simulation.
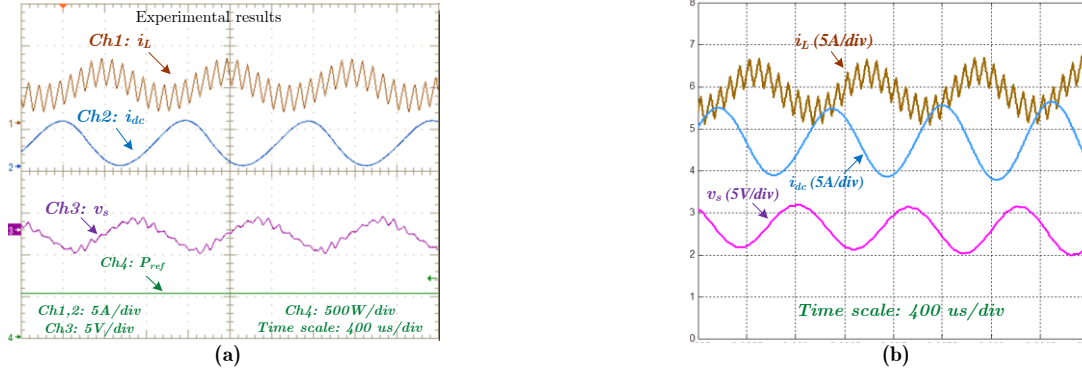

Fig. 16. Current and voltage waveforms for the second scenario ($K_x = 1000$), with $P = 520W$, $K_{stab} = 0$, (a) experiment; (b) simulation.
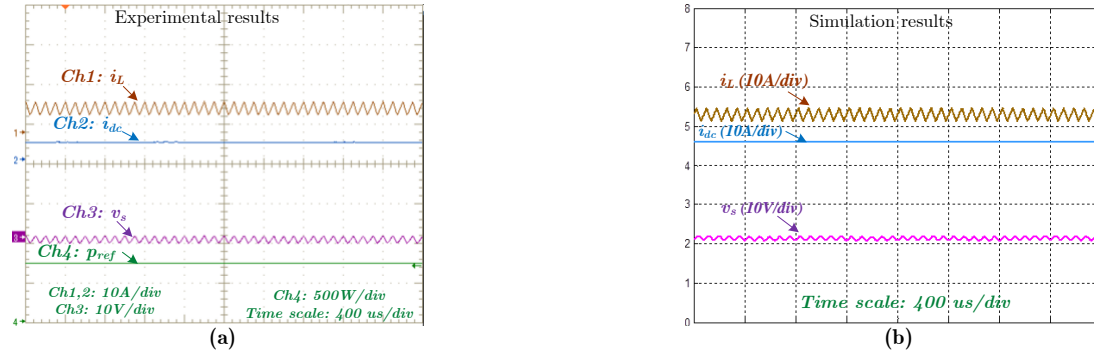

Fig. 17. Current and voltage waveforms for the third scenario ($K_x = 2200$), with $P = 740W$, $K_{stab} = 0$, (a) experiment; (b) simulation.
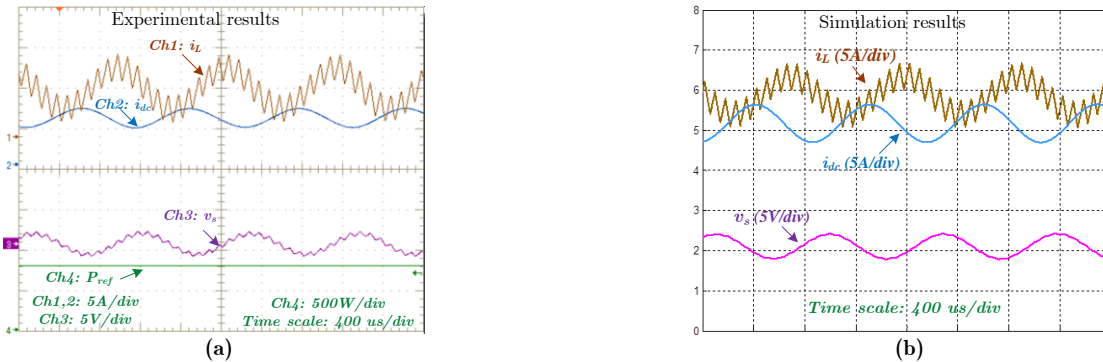

Fig. 18. Current and voltage waveforms for the third scenario ($K_x = 2200$), with $P = 800W$, $K_{stab} = 0$, (a) experiment; (b) simulation.
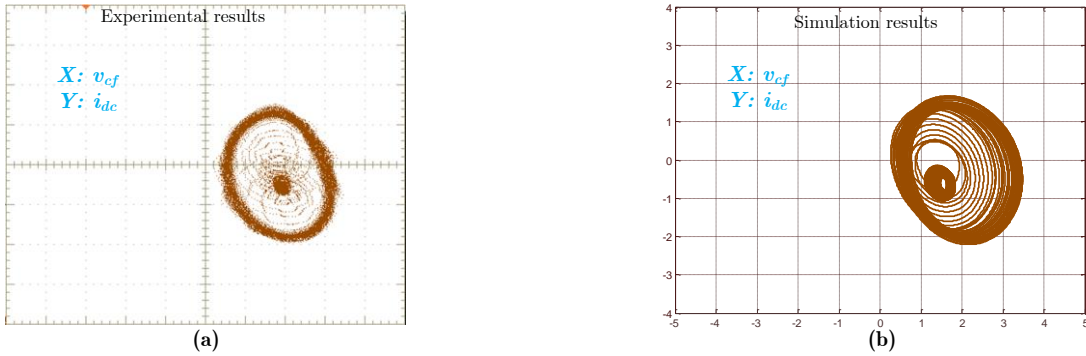
Fig. 19. Phase portrait of the state variables v_{cf} and i_{dc}, without stabilizer ($K_{stab} = 0$): (a) with experimental data; (b) simulation result.
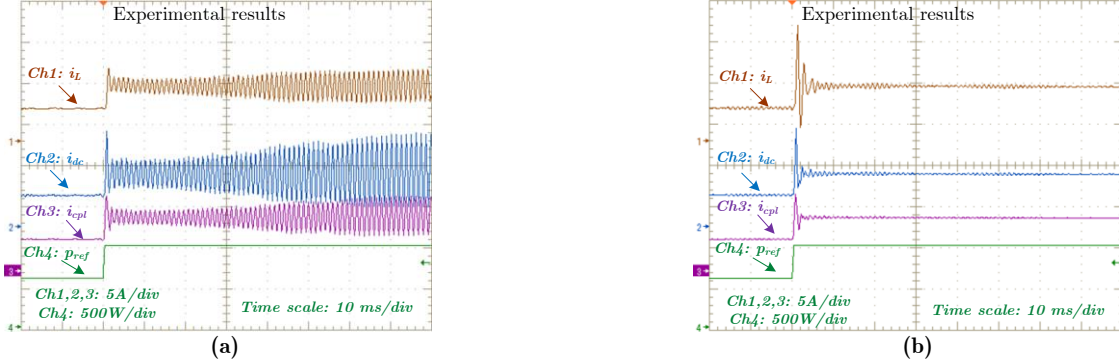

Fig. 20. System response $P = 600W \rightarrow 1000W$, $K_x = 2000$ (a) without stabilizer ($K_{stab} = 0$); (b) with stabilizer ($K_{stab} = 6.3$).

In the third scenario, tests were performed with $K_x = 2200$. The experimental current and voltage waveforms are presented in Fig. 17 (a), with $P = 740\ W$. The simulation waveforms for the same scenario are shown in Fig. 17 (b). The power was then increased to $800\ W$, as indicated in Fig. 18. The system loses stability as the power increases. This validates the theoretical results presented in Fig. 11.

For the first scenario, phase portraits are also constructed using both the experimental and simulation results, indicating the trajectory of the state variables v_{cf} and i_{dc} with change of the load power P. In Fig. 19 (a), the experimentally generated phase portrait of the system variables is presented, in which P is changed stepwise by $= 650W \rightarrow 900\ W$; Fig. 19 (b) shows the simulation results for the same scenario. As expected from the theoretical analysis, the system trajectory moves from a stable equilibrium point to unstable limit cycle oscillations.

TABLE II
RESULTS OF DIFFERENT EXPERIMENTAL SCENARIOS

K_x	Operating point				
	P=520W	P=650W	P=700W	P=740W	P=800W
1000	Unstable	Unstable	Unstable	Unstable	Unstable
2000	Stable	Stable	Unstable	Unstable	Unstable
2200	Stable	Stable	Stable	Stable	Unstable

B.   Dynamic Behavior of the System With Stabilizer

As the next step of experiments, the performance of the stabilizer is evaluated under a large change in the load power. Fig. 20 (a) indicates the system response when the load power changes stepwise from $P = 600\ W$ to $P = 1000\ W$, without using the stabilization system ($K_{stab} = 0$), and with $K_x = 2000$. The reference power is shown by the green line. The system loses stability, by increasing the CPL power. An experiment of the same scenario is then performed with

stabilizer's gain set to $K_{stab} = 6.3$, and the system currents are presented in Fig. 20 (b). It is observed that the system remains stable after increasing the load power. Therefore, the system can supply the higher amount of power to CPL. This was predicted by the proposed method in the stability map of Fig. 9. The transient behavior of the stabilizer is not the focus of this work. However, by using the selected stabilizer gain, the transient response of the control system is acceptable.

These laboratory tests verify the critical powers and the stability region, which were identified by the proposed discrete-time method in the different case studies. Limit cycle oscillations were observed in the characteristics of the system, including its currents and voltages, as predicted by the bifurcation analysis. The experimental waveforms are also consistent with those of time-domain simulation. However, slight differences are seen in frequency and magnitude of the oscillations compared to the simulation results. These differences can most likely be the result of the parasitic elements which are not considered in the simulation model.

VI. CONCLUSION

In this paper, a new discrete-time modeling for PWM converters is proposed which enables the stability analysis of DC distribution systems with nonlinear properties. One major advantage of this method is that it enables the switching effect to be considered using a general and simple discretization method. The proposed stability tool is able to identify slow scale and fast scale instabilities, which occur usually at high resonant frequencies. This instability cannot be detected with standard methods based on the conventional averaged model, because the switching effect is neglected in this model, and hence, the performance of averaging methods is influenced by the filter frequency and the dynamics of the system. By

contrast, the model proposed here can describe the dynamic properties of the system in a wide range of operations, independent of frequency. In the proposed discretization technique, the control command is assumed to change at an unknown instant; therefore, the performance of the model does not depend on the type of controller (i.e. digital or analog).

According to the proposed method, bifurcation diagrams were used to analyze the dynamic behavior of the system and the eigenvalues of the Jacobian matrix were calculated to study the stability of the system. The stability analysis of the system, resulting from the discrete-time method, was then validated experimentally. The experimental results are consistent with the results of the system analysis, as well as with the time-domain simulations. These experiments prove that the proposed method provides an accurate measure of the stability region of the DC distribution system. Therefore, instead of trial and error, the proposed method can be applied both to predict the instabilities and to guarantee the stability of the system during the design process. The proposed method can replace the conventional model in high frequency applications and can be generalized to different types of PWM converters.

Moreover, an active stabilizer has been included in the system model, in order to increase the stability margin of the system. The proposed discrete-time method has been used to investigate the sensitivity of the system's state to the parameter changes. The robustness of the stabilizer was then studied against the variation of the filter parameters. To this end, the performance of the stabilizer was validated by the experimental tests. We next hope to generalize the proposed stability tool to larger AC/DC microgrids.

REFERENCES

[1] D. Boroyevich, I. Cvetkovic, D. Dong, R. Burgos, F. Wang, and F. Lee, "Future electronic power distribution systems a contemplative view," in *Proc. 12th Int. Conf. Opt. Electric. & Electron. (OPTIM),* 2010, pp. 1369-1380.

[2] R. S. Balog and P. T. Krein, "Bus selection in multibus DC microgrids," *IEEE Trans. Power Electron.,* vol. 26, pp. 860-867, 2011.

[3] J. D. Dasika, B. Bahrani, M. Saeedifard, A. Karimi, and A. Rufer, "Multivariable control of single-inductor dual-output buck converters," *IEEE Trans. Power Electron.*, vol. 29, pp. 2061-2070, 2014.

[4] A. Kwasinski, "Quantitative evaluation of DC microgrids availability: Effects of system architecture and converter topology design choices," *IEEE Trans. Power Electron.,* vol. 26, pp. 835-851, 2011.

[5] P. C. Loh, D. Li, Y. K. Chai, and F. Blaabjerg, "Autonomous operation of hybrid microgrid with AC and DC subgrids," *IEEE Trans. Power Electron.,* vol. 28, pp. 2214-2223, 2013.

[6] A. Khaligh, "Realization of parasitics in stability of DC–DC converters loaded by constant power loads in advanced multiconverter automotive systems," *IEEE Trans. Ind. Electron.,* vol. 55, pp. 2295-2305, 2008.

[7] M. K. Zadeh, B. Zahedi, M. Molinas, and L. E. Norum, "Centralized stabilizer for marine DC microgrid," in *Proc. 39th Annual Conf. IEEE Ind. Electron. Society, IECON 2013*, 2013, pp. 3359-3363.

[8] H. Zhang, F. Mollet, C. Saudemont, and B. Robyns, "Experimental validation of energy storage system management strategies for a local dc distribution system of more electric aircraft," *IEEE Trans. Ind. Electron.,* vol. 57, pp. 3905-3916, 2010.

[9] C. Tse, "Chaos from a buck switching regulator operating in discontinuous mode," *Int. J. Circ. Theor. App.,* vol. 22, pp. 263-278, 1994.

[10] B. Basak and S. Parui, "Exploration of bifurcation and chaos in buck converter supplied from a rectifier," *IEEE Trans. Power Electron.,* vol. 25, pp. 1556-1564, 2010.

[11] M. K. Zadeh, G.-G. Roghayeh, S. Pierfederici, N.-M. Babak, and M. Molinas, "A new discrete-time modelling of PWM converters for stability analysis of DC microgrid," in *Proc. 11th Int. Conf. Modelling Simulation. Electric Machin., Converter. Syst.(Electrimacs'14)*, 2014.

[12] A. Emadi, A. Khaligh, C. H. Rivetta, and G. A. Williamson, "Constant power loads and negative impedance instability in automotive systems: definition, modeling, stability, and control of power electronic converters and motor drives," *IEEE Trans. Veh. Tech.,* vol. 55, pp. 1112-1125, 2006.

[13] A. Emadi, B. Fahimi, and M. Ehsani, "On the concept of negative impedance instability in the more electric aircraft power systems with constant power loads," *SAE Technical Paper*, 1999.

[14] A. M. Rahimi and A. Emadi, "An analytical investigation of dc/dc power electronic converters with constant power loads in vehicular power systems," *IEEE Trans. Veh. Tech.,*vol. 58, pp. 2689-2702, 2009.

[15] N. Bottrell, M. Prodanovic, and T. C. Green, "Dynamic stability of a microgrid with an active load," *IEEE Trans. Power Electron.,* vol. 28, pp. 5107-5119, 2013.

[16] M. Karbalaye Zadeh, M. Amin, J. A. Suul, M. Molinas, and O. B. Fosso, "Small-signal stability study of the Cigré DC grid test system with analysis of participation factors and parameter sensitivity of oscillatory modes " in *Proc. 18th Power Syst. Comput. Conf. (PSCC'14)*, Wroclaw, Poland, 2014.

[17] A. Kwasinski and C. N. Onwuchekwa, "Dynamic behavior and stabilization of DC microgrids with instantaneous constant-power loads," *IEEE Trans. Power Electron.,* vol. 26, pp. 822-834, 2011.

[18] D. Marx, P. Magne, B. Nahid-Mobarakeh, S. Pierfederici, and B. Davat, "Large signal stability analysis tools in DC power systems with constant power loads and variable power loads; a review," *IEEE Trans. Power Electron.,* vol. 27, pp. 1773-1787, 2012.

[19] M. Belkhayat, R. Cooley, and A. Witulski, "Large signal stability criteria for distributed systems with constant power loads," *in Proc. PESC'95,* pp. 1333-1338, 1995.

[20] W. Du, J. Zhang, Y. Zhang, and Z. Qian, "Stability criterion for cascaded system with constant power load," *IEEE Trans. Power Electron.,* vol. 28, pp. 1843-1851, 2013.

[21] A. Griffo and J. Wang, "Large signal stability analysis of more electric aircraft power systems with constant power loads," *IEEE Trans. Aero. Electron. Syst.,* vol. 48, pp. 477-489, 2012.

[22] S. Sanchez, R. Ortega, R. Grino, G. Bergna, and M. Molinas, "Conditions for existence of equilibria of systems with constant power loads," *IEEE Trans. Circuits Syst. I,* vol. 61, pp. 2204-2211, 2014.

[23] J. Sun and H. Grotstollen, "Symbolic analysis methods for averaged modeling of switching power converters," *IEEE Trans. Power Electron.,* vol. 12, pp. 537-546, 1997.

[24] A. Davoudi, J. Jatskevich, and T. De Rybel, "Numerical state-space average-value modeling of PWM DC-DC converters operating in DCM and CCM," *IEEE Trans. Power Electron.,* vol. 21, pp. 1003-1012, 2006.

[25] B. Lehman and R. M. Bass, "Switching frequency dependent averaged models for PWM DC-DC converters," *IEEE Trans. Power Electron.,* vol. 11, pp. 89-98, 1996.

[26] R. D. Middlebrook, "Input filter considerations in design and application of switching regulators," *in Proc. IAS'76,* 1976.

[27] F. Xiaogang, L. Jinjun, and F. C. Lee, "Impedance specifications for stable DC distributed power systems," *IEEE Trans. Power Electron.,* vol. 17, pp. 157-162, 2002.

[28] C. M. Wildrick, F. C. Lee, B. H. Cho, and B. Choi, "A method of defining the load impedance specification for a stable distributed power system," *IEEE Trans. Power Electron.,* vol. 10, pp. 280-285, 1995.

[29] S. D. Sudhoff and J. M. Crider, "Advancements in generalized immittance based stability analysis of DC power electronics based distribution systems," *in Proc. IEEE Electric Ship Tech. Symp.*, pp. 207-212, 2011.

[30] J. Sun, "Small-signal methods for AC distributed power systems–a review," *IEEE Trans. Power Electron.,* vol. 24, pp. 2545-2554, 2009.

[31] C. Wan, M. Huang, C. K. Tse, S. C. Wong, and X. Ruan, "Nonlinear behavior and instability in a three-phase boost rectifier connected to a nonideal power grid with an interacting load," *IEEE Trans. Power Electron.*, vol. 28, pp. 3255-3265, 2013.

[32] S. K. Mazumder, A. H. Nayfeh, and D. Boroyevich, "Theoretical and experimental investigation of the fast-and slow-scale instabilities of a dc-dc converter," *IEEE Trans. Power Electron.,* vol. 16, pp. 201-216, 2001.

[33] T. Geyer, G. Papafotiou, and M. Morari, "Hybrid model predictive control of the step-down DC-DC converter," *IEEE Trans. Control Syst. Tech.,* vol. 16, pp. 1112-1124, 2008.

[34] T. Geyer, G. Papafotiou, R. Frasca, and M. Morari, "Constrained optimal control of the step-down DC–DC converter," *IEEE Trans. Power Electron.,* vol. 23, pp. 2454-2464, 2008.

[35] S. K. Mazumder, A. H. Nayfeh, and D. Boroyevich, "An investigation into the fast-and slow-scale instabilities of a single phase bidirectional boost converter," *IEEE Trans. Power Electron. ,* vol. 18, pp. 1063-1069, 2003.

[36] D. Maksimovic and R. Zane, "Small-signal discrete-time modeling of digitally controlled PWM converters," *IEEE Trans. Power Electron.,* vol. 22, pp. 2552-2556, 2007.

[37] A. El Aroudi, B. G. M. Robert, A. Cid-Pastor, and L. Martínez-Salamero, "Modeling and design rules of a two-cell buck converter under a digital PWM controller," *IEEE Trans. Power Electron.,* vol. 23, pp. 859-870, 2008.

[38] S. Maity, "Dynamics and stability issues of a discretized sliding-mode controlled DC-DC buck converter governed by fixed-event-time switching," *IEEE Trans. Circuits Syst. I,* vol. 60, pp. 1657-1669, 2013.

[39] X. Wu, G. Xiao, and B. Lei, "Simplified discrete-time modeling for convenient stability prediction and digital control design," *IEEE Trans. Power Electron.,* vol. 28, pp. 5333-5342, 2013.

[40] A. H. Nayfeh and B. Balachandran, *Applied nonlinear dynamics: analytical, computational and experimental methods*, John Wiley & Sons, 2008.

[41] C. K. Tse, *Complex behavior of switching power converters*, CRC press, 2003.

[42] M. Cespedes, X. Lei, and J. Sun, "Constant-power load system stabilization by passive damping," *IEEE Trans. Power Electron.,* vol. 26, pp. 1832-1836, 2011.

[43] L. Wook-Jin and S. Seung-Ki, "DC-Link voltage stabilization for reduced DC-link capacitor inverter," *IEEE Trans. Ind. App.,* vol. 50, pp. 404-414, 2014.

[44] P. Magne, D. Marx, B. Nahid-Mobarakeh, and S. Pierfederici, "Large-signal stabilization of a DC-link supplying a constant power load using a virtual capacitor: impact on the domain of attraction," *IEEE Trans. Ind. App.,* vol. 48, pp. 878-887, 2012.

[45] P. Magne, B. Nahid-Mobarakeh, and S. Pierfederici, "General active global stabilization of multiloads DC-power networks," *IEEE Trans. Power Electron.,* vol. 27, pp. 1788-1798, 2012.

[46] E. Jamshidpour, B. Nahid-Mobarakeh, P. Poure, S. Pierfederici, F. Meibody-Tabar, and S. Saadate, "Distributed active resonance suppression in hybrid DC power systems under unbalanced load conditions," *IEEE Trans. Power Electron.,* vol. 28, pp. 1833-1842, 2013.

[47] E. Monmasson, *Power Electronic Converters: PWM Strategies and Current Control Techniques*, John Wiley & Sons, 2013.

[48] O. Lopez Santos, L. Martinez-Salamero, G. Garcia, H. Valderrama-Blavi, and T. Sierra-Polanco, "Robust control design for a voltage regulated quadratic boost converter," *IEEE Trans. Power Electron.,* vol. 30, pp. 2313-2327, 2015.

[49] R. Priewasser, M. Agostinelli, C. Unterrieder, S. Marsili, and M. Huemer, "Modeling, control, and implementation of DC–DC converters for variable frequency operation," *IEEE Trans. Power Electron.,* vol. 29, pp. 287-301, 2014.

[50] A. Lachichi, S. Pierfederici, J. P. Martin, and B. Davat, "Study of a hybrid fixed frequency current controller suitable for DC-DC applications," *IEEE Trans. Power Electron.,* vol. 23, pp. 1437-1448, 2008.

[51] S. Banerjee and G. C. Verghese, *Nonlinear phenomena in power electronics*, IEEE, 1999.

Mehdi Karbalaye Zadeh (S'12) received the M.Sc. degree in electrical engineering from University of Tehran, Tehran, Iran, in 2010. He is currently working toward the PhD degree at the Department of Electric Power Engineering, Norwegian University of Science and Technology (NTNU), Trondheim, Norway. His research interests include control and stability analysis of power electronic systems, smart grid, and DC power distribution.

Roghayeh Gavagsaz-Ghoachani received the M.Sc. degree from the Institut National Polytechnique de Lorraine (INPL), Nancy, France, in 2007, and the Ph.D. degree from the Université de Lorraine, France, in 2012, all in electrical engineering. She is researcher in the "Groupe de Recherche en Electrotechnique et Electronique de Nancy" (GREEN) and also an Associate Professor in the Department of Renewable Energies, Shahid Beheshti University, Tehran. Her current research interests include the stability study and control of power electronics systems.

Jean-Philippe Martin is graduated from the University of Nancy, France. He received the Ph.D. degree from INP Lorraine, France, in 2003. Since 2004, he has been engaged as assistant professor at INPL. His research activities in GREEN, UMR/CNRS, include electrical machine controls, static converter architectures and their interactions with new electrical devices (fuel cell and photovoltaic system).

Serge Pierfederici received the Dipl.-Ing. degree in electrical engineering from the Ecole Nationale Supérieure d'Electricité et de Mécanique (ENSEM) of Institu National Polytechnique de Lorraine (INPL), Nancy, France, in 1994, and the Ph.D. degree from the Institut National Polytechnique de Lorraine (INPL), Nancy, in 1998. Since 1999, he has been with INPL, where he is currently a Full Professor. His research interests include stability study of distributed power systems and modeling and control of power electronic converters.

Babak Nahid-Mobarakeh (M'05, SM'12) received the Ph.D. degree from "Institut National Polytechnique de Lorraine" (INPL) in 2001 in electrical engineering. From 2001 to 2006, he was with the "Centre de Robotique, Electrotechnique et Automatique", Amiens, France, as an Assistant Professor at the University of Picardie. In September 2006, he joined the "Ecole Superieure d'Electricite et de Mecanique" at the University of Lorraine where he is now an Associate Professor. He is also with the Groupe de Recherche en Electrotechnique et Electronique de Nancy (GREEN). He is the author or coauthor of more than 100 international journals and conference papers. His main research interests include nonlinear and robust control techniques applied to electric systems, fault detection and fault tolerant control of power systems, and stabilization of microgrids.

Marta Molinas (M'94) received the Diploma degree in electromechanical enginee ring from the National University of Asuncion, Asuncion, Paraguay, in 1992; the Master of Engineering degree from Ryukyu University, Okinawa, Japan, in 1997; and the Doctor of Engineering degree from the Tokyo Institute of Technology, Tokyo, Japan, in 2000. She was a Guest Researcher with the University of Padova, Padova, Italy, during 1998. From 2004 to 2007, she was a Postdoctoral Researcher with the Norwegian University of Science and Technology (NTNU) and from 2008-2014 she has been professor at the Department of Electric Power Engineering at the same university. In 2014, she was with Columbia University working with microgrids for developing regions. She is currently at the Department of Engineering Cybernetics, NTNU, as a Full Professor. From 2008 to 2009, she was a Japan Society for the Promotion of Science (JSPS) Research Fellow for ten months with the Energy Technology Research Institute, National Institute of Advanced Industrial Science and Technology, Tsukuba, Japan. Her research interests include stability of power electronics systems, harmonic and oscillatory phenomena, non-stationary signals from human and machines. Dr. Molinas has been an AdCom Member of the IEEE Power Electronics Society. She is actively engaged as a Reviewer for IEEE TRANSACTIONS ON INDUSTRIAL ELECTRONICS and IEEE TRANSACTIONS ON POWER ELECTRONICS.